

## Shoreline Extraction Based on LiDAR Data Obtained Using an USV

A. Halicki<sup>1,2</sup>, M. Specht<sup>1,3</sup>, A. Stateczny<sup>4</sup>, C. Specht<sup>3</sup> & O. Lewicka<sup>3</sup>

<sup>1</sup> Marine Technology Ltd., Gdynia, Poland

<sup>2</sup> University of Porto, Porto, Portugal

<sup>3</sup> Gdynia Maritime University, Gdynia, Poland

<sup>4</sup> Gdańsk University of Technology, Gdańsk, Poland

**ABSTRACT:** This article explores the use of Light Detection And Ranging (LiDAR) derived point clouds to extract the shoreline of the Lake Kłodno (Poland), based on their geometry properties. The data collection was performed using the Velodyne VLP-16 laser scanner, which was mounted on the HydroDron Unmanned Surface Vehicle (USV). A modified version of the shoreline extraction method proposed by Xu et al. was employed, comprising of the following steps: (1) classifying the point cloud using the Euclidean cluster extraction with a tolerance parameter of 1 m and min. cluster size of 10,000 points, (2) further filtration of boundary points by removing those with height above 1 m from the measured elevation of water surface, (3) manual determination of a curve consisting of 5 points located along the entire shoreline extraction region at a relatively constant distant from the coast, (4) removal of points that are further from the curve than the average distance, repeated twice. The method was tested on the scanned section of the lake shoreline for which Ground Control Points (GCP) were measured using a Global Navigation Satellite System (GNSS) Real Time Kinematic (RTK) receiver. Then, the results were compared to the ground truth data, obtaining an average position error of 2.12 m with a standard deviation of 1.11 m. The max error was 5.54 m, while the min. error was 0.41 m, all calculated on 281 extracted shoreline points. Despite the limitations of this parametric, semi-supervised approach, those preliminary results demonstrate the potential for accurate shoreline extraction based on LiDAR data obtained using an USV. Further testing and optimisation of this method for larger scale and better generalisation for different waterbodies are necessary to fully assess its effectiveness and feasibility. In this context, it is essential to develop computationally efficient methods for approximating shorelines that can accurately determine their course based on a set of points.

### 1 INTRODUCTION

A shoreline is a boundary between the land and water surfaces [1]. It is characterised by instability and functional diversity which vary depending on the region [2]. This boundary is of particular importance from the perspective of economic and environmental policies of the coastal states. This stems from the fact that the shoreline is rich in natural resources, which is why approx. 50% of the world's population inhabits the areas located within 100 km of the shoreline [1].

Therefore, it is essential to monitor the state of the seashore, which changes rapidly and is determined by numerous anthropogenic and natural factors. These include: biological activity, coastal flooding [3], earthquakes [4], marine erosion, ocean acidification [5], ocean currents, river regulation, sea level rise [6], seawater intrusion [7], temperature increase, tides, transportation of the rock debris [8] or wave action. Research into the impact of the above-mentioned factors on the shoreline course is conducted in a variety of waterbodies such as bays [9], river deltas

and estuaries [10,11], wetlands [12], as well as other geographic formations situated along the coast [13,14]. Due to complex shoreline dynamics, different indicators [e.g. High Water Line (HWL), Mean High Water Line (MHWL)] are used to define and describe shoreline [1]. Moreover, different authors often use divergent definitions for the same shoreline indicators [1].

Similarly, many different methods for determining the shoreline course are applied throughout the literature. These include: geodetic surveys [15,16], in particular, those using the Global Positioning System (GPS) and remote sensing measurements [17] performed using unmanned and manned airborne systems [18], as well as satellites [19]. In recent years, Light Detection And Ranging (LiDAR) has become a popular method for shoreline determination. LiDAR measurements are typically performed using airborne systems [13], and allow for a large area to be covered in a relatively short time [20,21]. The method involves emitting a beam of light at a specific wavelength and recording the return signal if the beam encounters a reflector (i.e., a light reflecting object). By measuring the time, it takes for the beam to return and taking into account the device's orientation in space and the angle at which the beam was emitted, it is possible to calculate the position of the reflector. LiDAR has several advantages over other shoreline determination methods, including its ability to capture detailed topographic information, its high accuracy and precision, as well as its ability to provide data in real-time [22]. However, the use of LiDAR also has its limitations, including relatively high cost, the need for extensive data pre-processing, as well as dependence on environmental and weather conditions, which can make LiDAR less practical for some applications.

Farris et al. [22] compared three shoreline extraction methods used by the United States Geological Survey (USGS) as part of the Marine Geology Program. The first of them is a modified profile method as described by [21]. It uses a 20 m-wide window determined along the transverse profiles. The second one is the grid method based on the interpolation of heights onto a grid of squares. The third one is a contour method that allows a contour of the Mean High Water (MHW) level to be obtained by using the contour generation function in the ArcGIS software. As part of the validation tests, a visual and quantitative assessment of the shoreline extraction accuracy was conducted based on the Airborne Laser Scanning (ALS) data recorded using the ATM-II system. The measurements were performed on Fire Island (USA) by the National Oceanic and Atmospheric Administration (NOAA) and the USGS in the years 2000 and 2012. The authors had no data on the actual position of the shoreline, which prevented the comparison of the errors in the determination of its course. For this reason, they decided to compare the differences in the extraction results between the individual methods. The authors quantitatively demonstrated that the shoreline courses obtained using the contour, grid and profile methods are very similar to each other, with shifts between them of less than 1 m.

Fernández Luque et al. [23] developed the Elevation Gradient Trend Propagation (EGTP) method for shoreline extraction, which uses the

iterative method based on a grid of squares. The EGTP method involves the use of the elevation gradient trend (its size and direction) calculated for each grid cell of a known elevation towards cells of an unknown elevation. This process is repeated until the new point of the grid reaches a level similar to (lower than) the selected vertical reference system. In this way, it is easy to determine the shoreline course from the extrapolated terrain model. As part of the validation tests, a visual and quantitative assessment of the shoreline extraction accuracy was conducted based on the ALS data recorded using the Leica Geosystems ALS60 system. The measurements were performed along the Mediterranean coast in the Almeria province (Spain) in 2009. The shoreline extraction errors were referred to 62 control points that were determined using a Differential Global Positioning System (DGPS) receiver. As demonstrated by statistical analyses, the mean uncertainty and the median uncertainty for the EGTP method were 2.08 m and 1.51 m, respectively. The study results obtained using the elevation gradient trend propagation were compared with the results obtained using the reference methods as proposed by [21,22]. The EGTP method has been proven to have a higher accuracy of the shoreline course determination than that of the reference methods.

Hua et al. [24] developed a method for detecting shores of an anthropogenic nature. At the beginning of the paper, attention was drawn to the large volume of data derived from LiDAR measurements. Therefore, the authors proposed simple criteria to limit the size of the LiDAR point cloud, thus reducing the computational complexity at the later stages of the anthropogenic method. External software was used for the visualisation and analysis of the LiDAR points. This enabled the determination of the coordinate range of the area under study, the coordinate range within which the shoreline is found, the scanning direction when using aircraft and the side on which the shoreline was located on the scan. The program also enabled the performance of preliminary segmentation (classification) of the area under study. Subsequently, the points that may have been reflected from the water surface were removed. Only then could the shoreline course be determined based on the information on the direction of flight. As part of the validation tests, a visual assessment of the shoreline extraction accuracy was conducted based on the ALS data. The measurements were conducted in the coastal zone of Longkou (China). The authors compared the method they had proposed with the contour method only visually. Unfortunately, they failed to describe the reference method.

Liu et al. [25] proposed two shoreline extraction methods, both of them using LiDAR data and remote sensing imagery. It is noteworthy that the authors created and made available a plugin for the ArcGIS software named "ShorelineExtractor", which enables the determination of the shoreline course using the contour and object-oriented methods. The contour method subtracts the elevation of the local tidal system from the elevation in the Digital Terrain Model (DTM). In this way, a contour (a shoreline) with an elevation of 0 m is obtained. On the other hand, in the object-oriented method, a cluster of land or water pixels is regarded as an object, while the

shorelines are created as boundaries between clusters of different classes. The "ShorelineExtractor" extension also enables the generalisation and smoothing of the shoreline obtained using one of the two methods proposed by the authors. The first of them is the shoreline simplification by the Douglas-Peucker method, which preserves points that are relevant in terms of maintaining the basic shape of the curve. The second method involves an analysis of the shoreline shape and the elimination of bends with high curvature. As part of the validation tests, a visual assessment of the shoreline extraction accuracy was conducted based on the ALS data recorded using the ATM system. The measurements were conducted in the coastal zone of Galveston Bay (USA) in 1999. The study demonstrated that the accuracy of the shoreline course determination was 4.5 m ( $p=0.95$ ). It should be pointed out that the use of a constant tidal datum value for a large region could lead to an error in shoreline position determination.

Xu et al. [26] proposed a parametric method of shoreline extraction based on the cloud of points surveyed by LiDAR. The first part of the algorithm involves the detection and rejection of the points belonging to the water surface by using plane fitting by the RANdom SAmple Consensus (RANSAC) method [29], as well as density and distance characteristics of individual points [30]. The second part of the algorithm involves classification of the land returns using the Euclidean cluster extraction [27,28]. The indication of potential boundary points and the optimisation of the boundary formed from them based on the cost function optimisation model [26,31]. As part of the validation tests, a visual and quantitative assessment of the shoreline extraction accuracy was conducted based on the ALS data. The measurements were carried out on five waterbodies with different geometrical and optical characteristics: Bowman Lake, Canyon Stream, Oregon Estuary, Susquehanna River and Wax Lake, in the years 2005–2014. Shoreline extraction accuracy metrics, such as correctness and completeness, were calculated as 90.7% and 92.5%, respectively. Moreover, it was demonstrated that the accuracy of the shoreline course determination by the parametric method on five different waterbodies was 1 m [26]. The obtained results were compared with the results presented in four different papers addressing similar issues. It has been proven that their accuracy level was 1.5–31 m, i.e. lower than that of the parametric method [26,32–35]. It should be noted that the extraction results were obtained on various data sets (aerial images and LiDAR points) with different spatial resolutions. The authors also addressed the issues related to the parametricity of the method proposed. The operation of the algorithm was tested for different parameter values. In their article, they provided suggested values of individual parameters for which satisfactory results of the shoreline extraction on five waterbodies were obtained.

Yousef et al. [36,37] developed a morphological shoreline extraction method, which uses a DTM created based on the ALS data and the local tidal system. The morphological algorithm comprises eight main stages. The first stage is the process of converting the point cloud from LiDAR measurements into the form of a digital terrain model.

In the second stage, the segmentation (classification) of each cell of the DTM to one of the two classes: land or water, is performed. In the third stage, the anomalies that are interpreted as outliers and measurement errors are detected and removed using the neighbourhood test. In the fourth stage, constrained morphological open and close operations are carried out in order to remove the remaining artifacts, such as gaps between the neighbouring land areas or broken parts of water areas. In the fifth stage, small isolated land and water bodies are removed. In the sixth stage, the Hough transform [38] is applied to remove structures of an anthropogenic nature, such as bridges, docks or fishing piers. In the seventh stage, the shoreline is determined and subsequently smoothed. To this end, the authors performed the Gaussian kernel. In the eighth stage, the shoreline obtained was superimposed on an aerial image in order to visually assess the extraction results. As part of the validation tests, a visual and quantitative assessment of the shoreline extraction accuracy was conducted based on the ALS data recorded using the LMS-Q680i system. The measurements were performed along the coast of the USA, passing through three states: New Jersey, Rhode Island and Virginia, in the years 2008–2012. In order to assess the shoreline extraction accuracy, the shoreline determined manually based on an aerial image was used. Moreover, a Monte Carlo simulation was performed in the article in order to estimate the shoreline extraction errors using the morphological method. Statistical analyses showed that the mean error and the standard deviation were 1.21 m and 1.97 m, respectively. The study results obtained using the morphological method were compared with the results obtained using the reference methods proposed by [25,39]. The morphological method has been proven to have a higher accuracy of shoreline position determination than that of the reference methods.

As part of the INNOBAT project [40], it was decided to implement the parametric method [26] for shoreline extraction. An important advantage of the method is the use of only the geometrical properties of the LiDAR point cloud. The method proposed enables the full automation of the extraction process and offers the possibility for conducting further research to attempt to develop specific parameter values for a particular measurement (waterbody type, the nature of the shoreline and measurement conditions) [31]. Moreover, according to the results presented by the original authors, the parametric method enables the fulfilment of the accuracy requirements provided for the most rigorous International Hydrographic Organization (IHO) order, i.e. the Exclusive Order (horizontal accuracy of 5 m ( $p=0.95$ )) [41], which refer to the works related to the shoreline course determination. In view of the above, the aim of this article is to validate the parametric method of shoreline extraction based on the LiDAR data recorded using an Unmanned Surface Vehicle (USV).

## 2 MATERIALS AND METHODS

### 2.1 Data collection

The shoreline extraction was performed on data collected with the Velodyne VLP-16 laser scanner mounted on the HydroDron USV. Obtained results were validated against the ground-truth data determined with a Global Navigation Satellite System (GNSS) Real Time Kinematic (RTK) receiver. The study area was a shoreline section of the Lake Kłodno (Poland). Both the lake and the measurement area are presented on Figure 1.



Figure 1. Satellite image of the Lake Kłodno with the area in which the hydrographic surveys were conducted marked with a red rectangle.

The data was collected and georeferenced to the PL- Universal Transverse Mercator (UTM) (zone 34N) and PL-EVRF2007-NH systems using the HYPACK software. To compensate for the movements of the vessel and obtain accurate positions, the HYPACK program was integrated with the Ekinox2-U Inertial Navigation System (INS) and a GNSS RTK receiver.

### 2.2 Shoreline extraction method

The shoreline extraction method used in this work is based on the method proposed by Xu et al. [26]. The modifications involve additional filtration steps and skipping of the shoreline approximation using the cost model proposed by the authors of the original method. This was due to the problems with the implementation of the original approach, described in further sections of the article. The shoreline extraction method used in this work comprises of five main stages:

1. Classification of points in the LiDAR derived point cloud into clusters using Euclidean clustering, described in detail by Rusu [28];
2. Indication of potential boundary points using the authors' original test algorithm [26];
3. Filtration of potential boundary points using the elevation threshold;
4. Manual indication of curve points in the water along the entire shoreline section at a relatively constant distance from the shore;
5. Calculation of the average distance between the points and the formed curve, rejection of points found further than the average distance.

### 2.3 Extraction error calculation

In order to quantitatively measure the error of the extraction method, the Euclidean distance was computed between coordinates of each extracted point and the coordinates of the closest Ground Control Point (GCP). The Mean Error (ME) was calculated using the Euclidean distance, and its formula is given by Equation 1:

$$ME = \frac{1}{N} \sum_{i=1}^N \min_j [d(P_i, GCP_j)], \quad (1)$$

where:

- $N$  – number of extracted shoreline points (-);
- $i$  – numbering representing shoreline points (-);
- $j$  – numbering representing GCPs (-);
- $P_i$  –  $i$ -th shoreline point (-);
- $GCP_j$  –  $j$ -th GCP (-);
- $d(P_i, GCP_j)$  – Euclidean distance between  $i$ -th shoreline point and  $j$ -th GCP (m).

The Euclidean distance for a pair of shoreline points  $p, q$  is given by Equation 2:

$$d(p, q) = \sqrt{(x_p - x_q)^2 + (y_p - y_q)^2 + (z_p - z_q)^2}, \quad (2)$$

where:

- $d(p, q)$  – Euclidean distance between points  $p, q$  in three- dimensional Cartesian coordinate space (m);
- $p, q$  – numbering representing a pair of shoreline points (-);
- $x$  – longitude of the shoreline point (m);
- $y$  – latitude of the shoreline point (m);
- $z$  – height of the shoreline point (m).

Min. and max values of the shoreline position error were calculated in similar manner, as well as the standard deviation of the mean. Obtained values are presented at the end of the Results section.

## 3 RESULTS

The shoreline extraction method applied was developed based on the extraction method proposed by Xu et al. [26]. Several issues that were described in detail in this article prevented the authors of this study from implementing the method described in [26] in its original form. Additional filtering steps were required in order to remove the excess points. Moreover, the method for shoreline approximation given a set of boundary points was not performed due to problems with its implementation. Instead, the manual connection of extracted points was performed for ease of visual analysis. Additionally, the mean shoreline position error and deviation were calculated. It should be also noted that the point cloud data used in this study was obtained using a different technique [Terrestrial Laser Scanning (TLS) from a moving USV rather than ALS]. Below are the results of the extraction routine performed in this paper. The following steps assume that the cloud does not contain many water returns. Otherwise, prior filtration of water returns should be performed, e.g. using the density and distance thresholds mentioned



by [26,30]. In the case of the measurements on the Lake Kłodno, there were hardly any water reflections, thus, the additional filtration step was not performed (Figure 2).

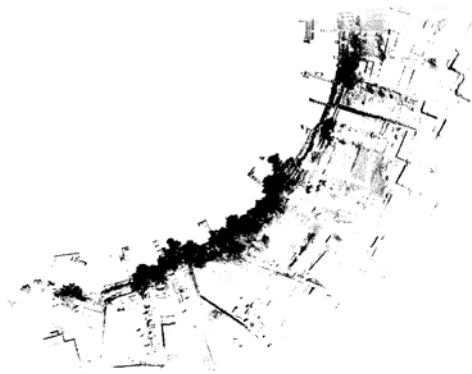


Figure 2. Point cloud derived from LiDAR measurements conducted along the section of the Lake Kłodno shoreline.

### 3.1 Clusterisation of LiDAR returns

One of the first steps of the algorithm is the Euclidean extraction, which clusters points in the point cloud based on the distance to others. This algorithm requires that three parameters are provided [28]. These are the min. number of points in the cluster, the max number of points in the cluster and the cluster tolerance. In their study, the authors [26] only provided the value used for the min. number of points in the cluster. The max number of points in the cluster can be omitted, by setting its value as the number equal to or higher than the number of points in the cloud. This was done in this study, as a result the constraint on the max cluster size was removed. However, the cluster tolerance parameter is crucial, affecting the results dramatically, yet it also remains left out in the study by Xu et al. [26]. The clusterisation step could be described as the data pre-processing stage and has a huge impact on the results of the rest of the algorithmic routine. It was necessary to determine the parameters of the clustering process for the study area. To this end, the Euclidean clustering [28] was performed for all the combinations of parameter values from Table 1. Results of the classification obtained for each parameter combination were evaluated through visual inspection.

Table 1. Parameter grid used for the Euclidean clustering evaluation.

Parameter	Value
Tolerance (m)	0.1, 0.25, 0.5, 0.75, 1, 1.5, 2, 3, 4
Min. points (-)	200, 10000
Max points (-)	$10^8$ (represents no restrictions)

Selected results from the Euclidean clustering are presented on Figures 3 and 4.

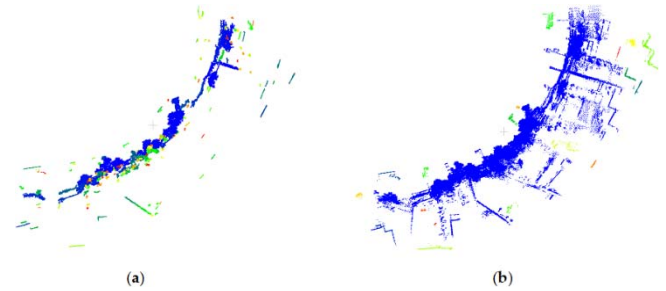


Figure 3. Influence of the tolerance parameter on the clusterisation results. The left image (a) shows the results of the Euclidean clustering with a tolerance of 0.25 m and min. cluster size set to 200 points. The right image (b) shows the results of the Euclidean clustering with a tolerance of 3 m and min. cluster size set to 200 points.

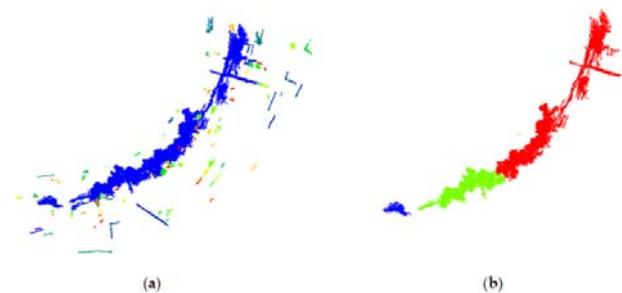


Figure 4. Influence of the min. number of points in the cluster on the clusterisation results. The left image (a) shows the results of the Euclidean clustering with a tolerance of 0.5 m and min. cluster size set to 200 points. The right image (b) shows the results of the Euclidean clustering with a tolerance of 0.5 m and min. cluster size set to 10,000 points.

### 3.2 Identification of potential boundary points

In [26], an algorithm called the testing algorithm was proposed by the authors to identify potential boundary points using an iterative convex hull fitting approach. The algorithm required a custom implementation as the source code was not provided in the original paper. Therefore, the algorithm was re-implemented, according to the description provided in [26]. To ensure correctness of the implementation, a simple validation was performed on an artificial set of 100 points (Figure 5).

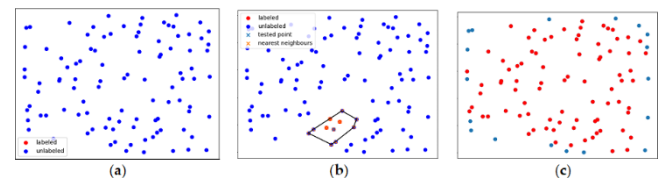


Figure 5. Testing algorithm [26] applied to an artificial set of 100 points. The left image (a) shows the initial stage of the algorithm when all points are treated as unlabeled potential candidates. In the middle plot (b), the first iteration of the algorithm is shown. For the first tested point, marked with a blue cross, 10 nearest neighbours are selected and marked with orange crosses. A convex hull is created for the set of points containing the tested point and its neighbours, marked by the black contour. The points inside the convex hull are labeled as non-boundary points and coloured red. The process is then repeated until no more points are found that could be labeled as non-boundary. The right image (c) shows the final results, where non-boundary points are coloured in red and potential boundary points are coloured in blue.

The results demonstrate that the testing algorithm was correctly implemented. Then, the algorithm was applied to the clustered point cloud to identify candidate boundary points for the Lake Kłodno dataset. Results of the boundary point identification using the testing algorithm [26] on real world LiDAR data are presented on Figure 6. They were obtained using the original point cloud with no downsampling, after performing the Euclidean clustering with a tolerance of 0.5 m and min. cluster size set to 10,000 points. In order to increase efficiency of the iterative convex hull fitting, a three-dimensional k-d tree [28] was used for space partitioning. Such approach is very efficient and may significantly speed up the process of searching nearest neighbours in the point cloud.

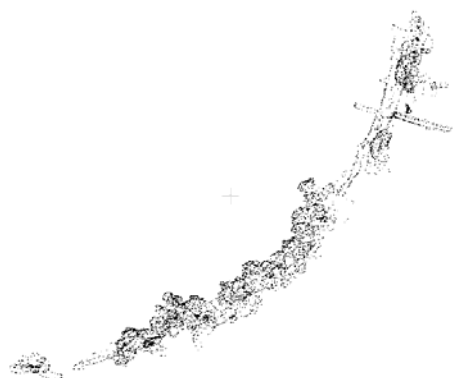


Figure 6. Results of the testing algorithm [26] applied to the Lake Kłodno dataset.

### 3.3 Filtration of potential boundary points

The main problem at this stage of the algorithm is to eliminate the points that do not constitute the shoreline (e.g. the tree cover). Including those points in the shoreline would greatly impact the accuracy. Therefore, a filtration method is necessary. To this end, the authors of the original method used an elevation threshold [26]. In this paper, the approach is followed, and the results of applying an elevation threshold of 1 m height relative to the measured water surface elevation are presented on Figure 7.

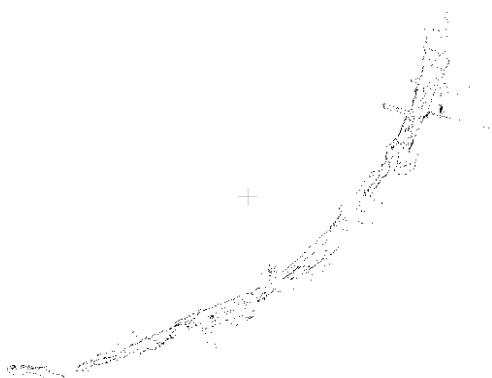


Figure 7. Results of filtration of the candidate point clouds using elevation threshold of 1 m height relative to the measured water surface elevation.

The above results are satisfactory, yet many points that are not direct components of the shoreline remain in the point cloud. Visual inspection of the point cloud at this stage revealed that some points in the cloud are up to 15–20 m inland. Therefore, another filtration was necessary. The filtration approach was based on the distance to the waterbody. To this end, the manual indication of a curve consisting of 5 points was performed. The curve was assumed to be placed on the waterbody and roughly following the shoreline. The elevation of the curve is constant and was determined by fitting a plane to all of the points remaining in the cloud. The mean Euclidean distance was calculated for all of the remaining potential boundary points. Then, the curve was used to filter out points that were further than mean distance from the curve. This was repeated twice, in order to strengthen the removal effect. The results of this supervised filtration approach are presented on Figure 8.

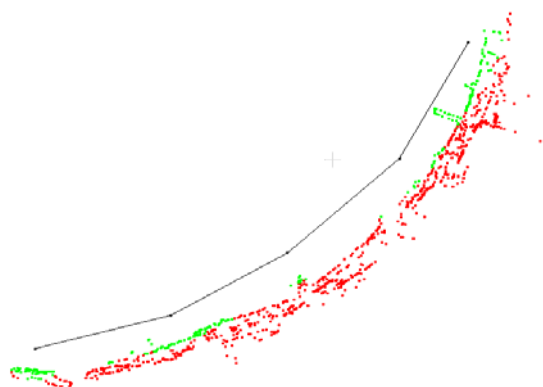


Figure 8. Results of filtration of the candidate point clouds using the mean distance from polyline threshold. Red points are removed from the candidate boundary points. Green points are the remaining points which will be used for boundary approximation. Two consecutive filtrations were performed using the same curve and shrinking set of candidate boundary points.

The elevation and waterbody distance filtration steps allowed to filter out the points that were deemed unnecessary, without losing the underlying shoreline geometry information. It should be noted that the shoreline is traditionally defined by a curve rather than a set of points. So far the algorithm results in a set of points. Therefore, it is necessary to determine an order in which the points should be connected. The approximation of shoreline from a set of points is a non-trivial task, which is described in-depth in the following section.

### 3.4 Approximation of shoreline from a set of points

Authors of the original article [26] propose to find the optimal shoreline from the set of boundary points by evaluating edges constructed by all possible 3-point permutations of said points. The paper proposes a cost optimisation model, which consists of nodes that represent the permutations. Single node in the model represents the selection of three points from the cloud and linking them as the leftmost, the middle and the rightmost one. The model evaluates each such

permutation using a novel cost function, which calculates the cost of each node according to the Equation 3 [26]:

$$\text{cost}(k,l,m) = \frac{d(k,l) + d(l,m)}{2} + \lambda \cdot \left| \cos\left(\frac{\theta_{klm}}{2}\right) \right|, \quad (3)$$

where:

$\text{cost}(k,l,m)$  – cost of the single node (-);

$k, l, m$  – numbering representing the  $k$ -th,  $l$ -th and  $m$ -th point from the point cloud (3-point permutation with no repetitions), assigned respectively as the leftmost, the middle and the rightmost points in the shoreline section (-);

$d(k,l)$  – Euclidean distance between the leftmost and the middle point in the node (m);

$d(l,m)$  – Euclidean distance between the middle and the rightmost point in the node (m);

$\lambda$  – weight coefficient (-);

$\theta_{klm}$  – angle between edges  $(k,l)$  and  $(l,m)$  (rad).

This is an NP-hard combinatorial optimisation problem. Solving such problems typically requires a specific approach that takes into account the problem's unique characteristics and structure. Due to the complexity of NP-hard problems, finding exact solutions may be infeasible or even impossible in some cases. Therefore, heuristic and approximation algorithms are often used to find near-optimal solutions efficiently. The authors [26] proposed to use a dynamic programming approach and backtrack the solution from the sink node to the source. However, the problem of defining source and sink nodes was not clearly addressed in their paper. The representation of the problem proposed by Xu et al. [26] is also computationally expensive. In a graph in which each node represents the 3-point permutation of points created from  $n$ -element point cloud, the number of permutations is described by Equation 4:

$$P(n,3) = \frac{1}{2} \cdot \frac{n!}{n-3}, \quad (4)$$

where:

$P(n,3)$  – set of all 3-element permutations with no repetitions from  $n$ -element point cloud (-);

$n$  – number of points in the point cloud (-).

Multiplication by  $\frac{1}{2}$  in the above formula results from ignoring reverse permutations. Point clouds derived from laser scanning are considerably large, and the number of points at the end of algorithmic routine may vary depending on the parameters an individual traits of the scanned area. For the dataset used in this study, after the elevation threshold there was still over 1000 points left, which results in over 840 million permutations with no repetitions and no reversed permutations included, according to the Equation 4. Due to the above-mentioned issues, the shoreline approximation based on the set of obtained boundary points was not performed in this study. Instead, a point-wise qualitative and quantitative error of shoreline extraction was performed. The extracted shoreline points (black colour) superimposed on the GCPs (green colour) are presented on Figure 9.

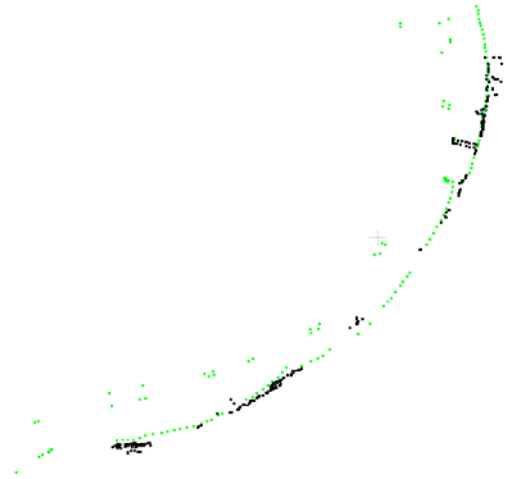


Figure 9. Extracted boundary points (black colour) superimposed on the GCPs (green colour).

In order to verify the performed extraction in a quantitative way, the position errors of the individual points making up the curve (shoreline) obtained were calculated. For each of the 281 shoreline points, the nearest GCP was selected. The calculated statistics are provided in Table 2.

Table 2. Summary of errors of the 281 points comprising the extracted shoreline obtained in relation to the reference line determined using a GNSS RTK receiver.

Mean error (m)	Standard deviation (m)	Max error (m)	Min. error (m)
2.12	1.11	5.54	0.41

A one-tailed t-test was additionally performed to verify, if the extraction results fulfil the accuracy requirements provided for the Exclusive Order (i.e. horizontal accuracy of 5 m ( $p=0.95$ )). In the test, the null hypothesis ( $H_0$ ) was specified as the (error) population mean being larger or equal to 5 m, while the alternative hypothesis ( $H_A$ ) was specified as the (error) population mean being less than 5 m. The calculated t-statistic of  $-43.36$  and a very small p-value of  $1.4 \cdot 10^{-126}$  m allow to reject the null hypothesis can be rejected with high confidence. Therefore, results presented in this work show that the method used fulfils the accuracy requirements provided for the most stringent IHO order.

## 4 DISCUSSION

Most of the state-of-the-art in the area of shoreline extraction puts focus on using methods based on DTMs using cross-shore profiles or contours of the vertical datums. This article explores the topic of shoreline extraction based on the geometry of LiDAR derived point clouds. Methods which are based solely on geometry are quite scarce in the literature. In this paper, the results of reimplementation of the method proposed by Xu et al. [26] are described. Specifically, the process of clustering the point cloud, identifying the candidate boundary points and filtering the candidates is validated on a real-world dataset.

The direct interpretation of the clusterisation results in the case of a problem with shoreline



identification is hindered due to the heterogeneity of the environment and the objects found there. In other words, this is not a pure test case of the desk object type [28], where the interpretation of the results is relatively easy. However, it is quite evident that the results are very parameter dependent. High tolerance values lead to grouping points into bigger clusters, while low values can separate too many clusters. Best results on the dataset from the Lake Kłodno were obtained for a tolerance of 0.5 m and min. cluster size of 10,000 points. These settings allowed for most of the point cloud to be discarded, while keeping the largest clusters adjacent to the waterbody. It is important to note that the results may differ if the point cloud was derived from ALS. Moreover, additional processing is needed to facilitate the task of shoreline identification with the resulting point cloud.

The iterative convex hull fitting approach is effective in identifying edges in an unorganised point cloud. However, although this approach significantly reduces the number of remaining points, further filtration is still required. It appears that this approach will inevitably result in a large number of points remaining at the far-off ends of the clusters, which need to be eliminated. To achieve this, the authors [26] employ an elevation threshold, which may pose challenges in areas with waterbodies that have varying elevations. Nevertheless, the original article demonstrates promising results in such cases. However, this approach may also prove challenging in areas with low terrain slopes surrounding the waterbody.

In this paper, a multi-step filtration approach was employed to identify shoreline points in a LiDAR derived point cloud. The first step involved using the elevation threshold as proposed by Xu et al. [26]. This approach is simple and effective, particularly in cases where only one waterbody is present in the scene and the adjacent terrain has a noticeable slope. However, in the case of the Lake Kłodno point cloud, this approach alone was not sufficient, and additional filtration was required due to the low terrain slope in the region. To address this issue, a supervised filtration step was proposed, which involved manually determining a 5-point curve that approximately followed the shoreline. Then, the mean distance from the curve was calculated for all remaining points and used as a threshold to eliminate far-off points that did not constitute the shoreline. This operation was repeated twice but could be repeated more times, though with increasing loss in the underlying shoreline geometry. This approach effectively removed unwanted points while preserving the essential shoreline points for further analysis.

The task of shoreline approximation is a complex one, as previously discussed. While the approach introduced by Xu et al. [26] of finding the min. cost path between permutations of all points in the point cloud is intriguing, its computational expense is a notable drawback. Moreover, the original manuscript lacked certain implementation details, which made reimplementing challenging. This emphasises the necessity of developing precise and efficient methods for approximating shorelines from point clouds.

## 5 CONCLUSIONS

The applied method successfully extracted the shoreline with an average accuracy of 2.12 m and a standard deviation of 1.11 m. However, to evaluate the method's reliability, it is essential to test it on larger data sets derived from diverse waterbodies and scanning techniques, such as ALS. Notably, Xu et al. [26] proposed their method for larger scale scenes surveyed using airborne LiDAR. This study demonstrates that key concepts utilised in the algorithmic routine, such as clusterisation, convex hull fitting, as well as elevation and distance thresholds, can effectively obtain a high accuracy shoreline representation that meets IHO standards. To utilise point cloud-based methods effectively, it is crucial to enhance filtration techniques and develop efficient algorithms for shoreline approximation. As the effectiveness of the investigated methods depends heavily on parameter settings, developing customisable plugins with user-friendly interfaces and interactive visualisations to assist in determining feasible parameters could be highly beneficial.

## FUNDING

This research was funded by the National Centre for Research and Development in Poland, grant number LIDER/10/0030/L-11/19/NCBR/2020. Moreover, this research was funded from the statutory activities of Gdynia Maritime University, grant numbers WN/PI/2023/03 and WN/2023/PZ/05.

## REFERENCES

1. Li, Z.; Zhai, J.; Wu, F. Shape Similarity Assessment Method for Coastline Generalization. *ISPRS Int. J. Geo-Inf.* 2018, 7, 283.
2. Sui, L.; Wang, J.; Yang, X.; Wang, Z. Spatial-temporal Characteristics of Coastline Changes in Indonesia from 1990 to 2018. *Sustainability* 2020, 12, 3242.
3. Kanwal, S.; Ding, X.; Sajjad, M.; Abbas, S. Three Decades of Coastal Changes in Sindh, Pakistan (1989–2018): A Geospatial Assessment. *Remote Sens.* 2020, 12, 8.
4. Nikolakopoulos, K.; Kyriou, A.; Koukouvelas, I.; Zygouri, V.; Apostolopoulos, D. Combination of Aerial, Satellite, and UAV Photogrammetry for Mapping the Diachronic Coastline Evolution: The Case of Lefkada Island. *ISPRS Int. J. Geo-Inf.* 2019, 8, 489.
5. Zhang, Y.; Hou, X. Characteristics of Coastline Changes on Southeast Asia Islands from 2000 to 2015. *Remote Sens.* 2020, 12, 519.
6. Mury, A.; Jeanson, M.; Collin, A.; James, D.; Etienne, S. High Resolution Shoreline and Shelly Ridge Monitoring over Stormy Winter Events: A Case Study in the Megatidal Bay of Mont-Saint-Michel (France). *J. Mar. Sci. Eng.* 2019, 7, 97.
7. Fu, Y.; Guo, Q.; Wu, X.; Fang, H.; Pan, Y. Analysis and Prediction of Changes in Coastline Morphology in the Bohai Sea, China, Using Remote Sensing. *Sustainability* 2017, 9, 900.
8. Mahamud, U.; Takewaka, S. Shoreline Change around a River Delta on the Cox's Bazar Coast of Bangladesh. *J. Mar. Sci. Eng.* 2018, 6, 80.
9. Martínez, C.; Quezada, M.; Rubio, P. Historical Changes in the Shoreline and Littoral Processes on a Headland Bay Beach in Central Chile. *Geomorphology* 2011, 135, 80–96.



10. Chu, Z.X.; Yang, X.H.; Feng, X.L.; Fan, D.J.; Li, Y.K.; Shen, X.; Miao, A.Y. Temporal and Spatial Changes in Coastline Movement of the Yangtze Delta during 1974–2010. *J. Asian Earth Sci.* 2013, 66, 166–174.
11. Cowart, L.; Corbett, D.R.; Walsh, J.P. Shoreline Change along Sheltered Coastlines: Insights from the Neuse River Estuary, NC, USA. *Remote Sens.* 2011, 3, 1516–1534.
12. Kuleli, T.; Guneroglu, A.; Karsli, F.; Dihkan, M. Automatic Detection of Shoreline Change on Coastal Ramsar Wetlands of Turkey. *Ocean Eng.* 2011, 38, 1141–1149.
13. Specht, M.; Specht, C.; Lewicka, O.; Makar, A.; Burdziakowski, P.; Dąbrowski, P. Study on the Coastline Evolution in Sopot (2008–2018) Based on Landsat Satellite Imagery. *J. Mar. Sci. Eng.* 2020, 8, 464.
14. Zhang, X.; Pan, D.; Chen, J.; Zhao, J.; Zhu, Q.; Huang, H. Evaluation of Coastline Changes under Human Intervention Using Multi-temporal High-resolution Images: A Case Study of the Zhoushan Islands, China. *Remote Sens.* 2014, 6, 9930–9950.
15. Specht, C.; Weintrit, A.; Specht, M.; Dąbrowski, P. Determination of the Territorial Sea Baseline—Measurement Aspect. *IOP Conf. Ser. Earth Environ. Sci.* 2017, 95, 1–10.
16. Specht, M.; Specht, C.; Wąż, M.; Dąbrowski, P.; Skóra, M.; Marchel, Ł. Determining the Variability of the Territorial Sea Baseline on the Example of Waterbody Adjacent to the Municipal Beach in Gdynia. *Appl. Sci.* 2019, 9, 3867.
17. Basterretxea, G.; Orfila, A.; Jordi, A.; Fornós, J.; Tintoré, J. Evaluation of a Small Volume Renourishment Strategy on a Narrow Mediterranean Beach. *Geomorphology* 2007, 88, 139–151.
18. Specht, M.; Specht, C.; Mindykowski, J.; Dąbrowski, P.; Maśnicki, R.; Makar, A. Geospatial Modeling of the Tombolo Phenomenon in Sopot Using Integrated Geodetic and Hydrographic Measurement Methods. *Remote Sens.* 2020, 12, 737.
19. Viaña-Borja, S.P.; Ortega-Sánchez, M. Automatic Methodology to Detect the Coastline from Landsat Images with a New Water Index Assessed on Three Different Spanish Mediterranean Deltas. *Remote Sens.* 2019, 11, 2186.
20. Boak, E.H.; Turner, I.L. Shoreline Definition and Detection: A Review. *J. Coast. Res.* 2005, 214, 688–703.
21. Stockdon, H.F.; Sallenger Jr., A.H.; List, J.H.; Holman, R.A. Estimation of Shoreline Position and Change Using Airborne Topographic Lidar Data. *J. Coast. Res.* 2002, 18, 502–513.
22. Farris, A.S.; Weber, K.M.; Doran, K.S.; List, J.H. Comparing Methods Used by the U.S. Geological Survey Coastal and Marine Geology Program for Deriving Shoreline Position from Lidar Data. Available online: <https://pubs.usgs.gov/of/2018/1121/ofr20181121.pdf> (accessed on 26 April 2023).
23. Fernández Luque, I.; Aguilar Torres, F.J.; Aguilar Torres, M.A.; Pérez García, J.L.; López Arenas, A. A New, Robust, and Accurate Method to Extract Tide-coordinated Shorelines from Coastal Elevation Models. *J. Coast. Res.* 2012, 28, 683–699.
24. Hua, L.W.; Bi, Y.L.; Hao, L. The Research of Artificial Shoreline Extraction Based on Airborne LIDAR Data. *J. Phys.: Conf. Ser.* 2021, 2006, 012048.
25. Liu, H.; Wang, L.; Sherman, D.J.; Wu, Q.; Su, H. Algorithmic Foundation and Software Tools for Extracting Shoreline Features from Remote Sensing Imagery and LiDAR Data. *J. Geogr. Inf. Syst.* 2011, 3, 99–119.
26. Xu, S.; Ye, N.; Xu, S. A New Method for Shoreline Extraction from Airborne LiDAR Point Clouds. *Remote Sens. Lett.* 2019, 10, 496–505.
27. Rusu, R.B. Semantic 3d Object Maps for Everyday Manipulation in Human Living Environments. *KI - Künstliche Intelligenz* 2010, 24, 345–348.
28. Rusu, R.B. Semantic 3d Object Maps for Everyday Manipulation in Human Living Environments. PhD Thesis, Technische Universität München, München, Germany, 2009.
29. Xu, S.; Xu, S. A Minimum-cost Path Model to the Bridge Extraction from Airborne LiDAR Point Clouds. *J. Indian Soc. Remote Sens.* 2018, 46, 1423–1431.
30. Smeckaert, J.; Mallet, C.; David, N.; Chéhata, N.; Ferraz, A. Large-scale Classification of Water Areas Using Airborne Topographic LiDAR Data. *Remote Sens. Environ.* 2013, 138, 134–148.
31. Lewicka, O.; Specht, M.; Stateczny, A.; Specht, C.; Dardanelli, G.; Brčić, D.; Szostak, B.; Halicki, A.; Stateczny, M.; Widźgowski, S. Integration Data Model of the Bathymetric Monitoring System for Shallow Waterbodies Using UAV and USV Platforms. *Remote Sens.* 2022, 14, 4075.
32. Di, K.; Wang, J.; Ma, R.; Li, R. Automatic Shoreline Extraction from High-resolution IKONOS Satellite Imagery. In Proceedings of the American Society for Photogrammetry and Remote Sensing Annual Conference 2003 (ASPRS 2003), Anchorage, AK, USA, 5–9 May 2003.
33. Lee, I.-C.; Cheng, L.; Li, R. Optimal Parameter Determination for Mean-shift Segmentation-based Shoreline Extraction Using Lidar Data, Aerial Orthophotos, and Satellite Imagery. In Proceedings of the American Society for Photogrammetry and Remote Sensing Annual Conference 2010 (ASPRS 2010), San Diego, CA, USA, 26–30 April 2010.
34. Liu, H.; Sherman, D.; Gu, S. Automated Extraction of Shorelines from Airborne Light Detection and Ranging Data and Accuracy Assessment Based on Monte Carlo Simulation. *J. Coast. Res.* 2007, 236, 1359–1369.
35. Niedermeier, A.; Romaneefsen, E.; Lehner, S. Detection of Coastlines in SAR Images Using Wavelet Methods. *IEEE Trans. Geosci. Remote Sens.* 2000, 38, 2270–2281.
36. Yousef, A.H.; Iftekharruddin, K.; Karim, M. A New Morphology Algorithm for Shoreline Extraction from DEM Data. In Proceedings of the SPIE Defense, Security, and Sensing 2013, Baltimore, MA, USA, 29–30 April 2013.
37. Yousef, A.H.; Iftekharruddin, K.M.; Karim, M.A. Shoreline Extraction from Light Detection and Ranging Digital Elevation Model Data and Aerial Images. *Opt. Eng.* 2013, 53, 011006.
38. Trucco, E.; Verri, A. *Introductory Techniques for 3-D Computer Vision*; Prentice Hall: Hoboken, NJ, USA, 1998.
39. Lee, I.-C.; Wu, B.; Li, R. Shoreline Extraction from the Integration of LiDAR Point Cloud Data and Aerial Orthophotos Using Mean Shift Segmentation. In Proceedings of the American Society for Photogrammetry and Remote Sensing Annual Conference 2009 (ASPRS 2009), Baltimore, MD, USA, 9–13 March 2009.
40. Specht, M.; Stateczny, A.; Specht, C.; Widźgowski, S.; Lewicka, O.; Wiśniewska, M. Concept of an Innovative Autonomous Unmanned System for Bathymetric Monitoring of Shallow Waterbodies (INNOBAT System). *Energies* 2021, 14, 5370.
41. IHO. *IHO Standards for Hydrographic Surveys*, 6th ed.; Special Publication No. 44; IHO: Monaco, Monaco, 2020.